Final Report: January, 1980-July, 1981

Grant: NASA-NAG1-33

SILICON SUPERLATTICES: THEORY AND APPLICATION TO SEMICONDUCTOR DEVICES

Principal Investigator: J.A. Moriarty+

College of William and Mary, Williamsburg, VA 23185

NASA Technical Officer: R.L. Stermer

NASA-Langley Research Center, Hampton, VA 23665

+Current address: Department of Electrical and Computer Engineering

University of Cincinnati

Cincinnati, Ohio 45221

(NASA-CR-164568) SILICON SUPERLATTICES: THEORY AND APPLICATION TO SEMICONDUCTOR DEVICES Final Report, Jan. 1980 - Jul. 1981 (College of William and Mary) 33 p HC A01/MF A01

N81-27949

CSCL 20L G3/76

Unclas 26841

I. INTRODUCTION

This report summarizes the research efforts of the principal investigator to initiate a theoretical study of silicon superlattices and their applicability to improved semiconductor devices. The work described here has proven to be very fruitful and is currently being continued by the author at this new institution, the University of Cincinnati. Additional support for this research, in the form of a separate NASA grant, is now pending.

The motivation for undertaking this investigation was two-fold. First, there has been a great deal of recent interest in the device-application potential of III-V semiconductor superlattices fabricated in the form of ultrathin (~100-500Å) periodically-layered heterostructures. This interest first began with the suggestion of Esaki and Tsu[1] that the atomic-like dimensions of such structures could lead to interesting and useful quantum size effects and would create the possibility of altering familiar transport and optical properties over broad physical ranges. The sophisticated technique of molecular-beam-epitaxy[2] has since been used to fabricate superlattices out of compatible semiconducting compounds and their alloys, most notably GaAs and $Ga_{1-x}Al_xAs$, where the lattice constants of the two constituents can be closely matched. Very recent research on the GaAs-$Ga_{1-x}Al_xAs$ system has been both intense and successful.[2-16] Applications to improved semiconductor lasers and electron devices have been achieved and many more are expected.

The second motivating ingredient for the present work was the natural question of whether or not such ideas had practical relevance to silicon, still the most technologically important electronic material. In particular, we were attracted by the prospect of combining the benefits of cost-effective materials processing, which is offered by current silicon technology, with the improved

electron-device performance promised by semiconductor superlattices. The modified electronic structure of the semiconductor superlattice brings with it the possibility of controlling basic electronic properties such as electron and hole mobilities. Of special interest is the possible application of silicon superlattices to faster high-speed computing devices, where one factor limiting the speed of the device is the relatively low carrier mobility in silicon.

Our specific objective during the first year was to investigate the modified electronic band structure of hypothetical silicon superlattice structures including, but not confined to, the heterostructure system of most direct interest: $Si\text{-}Si_{1-x}Ge_x$. Toward this end, we have now studied rather extensively three general prototype models of increasing complexity:

(i) a one-dimensional superlattice in an ideal one-dimensional model host: superlattice (1)

(ii) a two-dimensional superlattice in an ideal two-dimensional host: superlattice (2)

(iii) a one-dimensional superlattice in a real three-dimensional silicon host: superlattice (3)

In each case, we have examined in detail how the fundamental band gap, effective masses and related features of the electronic structure are altered from the host. These studies are discussed at length in Sec. II below. Our conclusions and suggestions for future directions are given in Sec. III.

II. COMPLETED RESEARCH

A. Electronic Structure of Model One-and Two-Dimensional Superlattices.

The model host in superlattices (1) and (2) was chosen to simulate a semiconductor like silicon yet retain a large degree of physical and mathematical simplicity. Conceptually, the superlattice is formed by substitutionally replacing host atoms by "impurity" atoms in a periodic fashion, where the underlying linear or square host crystal structure has a lattice constant a and two atoms per primative cell. The latter are separated by a distance d (the bond length). It is further assumed that the electron potential of the impurity atoms is characterized by a constant energy shift V_s from the host. Otherwise, the nature of the impurity atoms is arbitrary and need not be considered further. If the second atom in the primative cell is located at the point of highest symmetry, the geometry of superlattices (1) and (2) is specified by only two numbers: n_s, the total number of host primative cells (each with either 2 host or 2 impurity atoms) contained in a given (100) plane of the superlattice primative cell; and n_b, the number of those host primative cells which contain only impurity atoms. The geometry and electron potential of superlattice (1) are schematically illustrated in Fig. 1 for the case $n_s=3$ and $n_b=1$. Here

$$s=n_s a \tag{1}$$

is the lattice constant of the superlattice and

$$n_p=2n_s \tag{2}$$

is the number of atoms in the superlattice primative cell. In reciprocal space, the size of the Brillouin zone is correspondingly shrunk by a factor of n_s and the boundaries of the "minizone" for superlattice (1) are thus given by

$$\frac{-\pi}{s} \leq k \leq \frac{\pi}{s}. \tag{3}$$

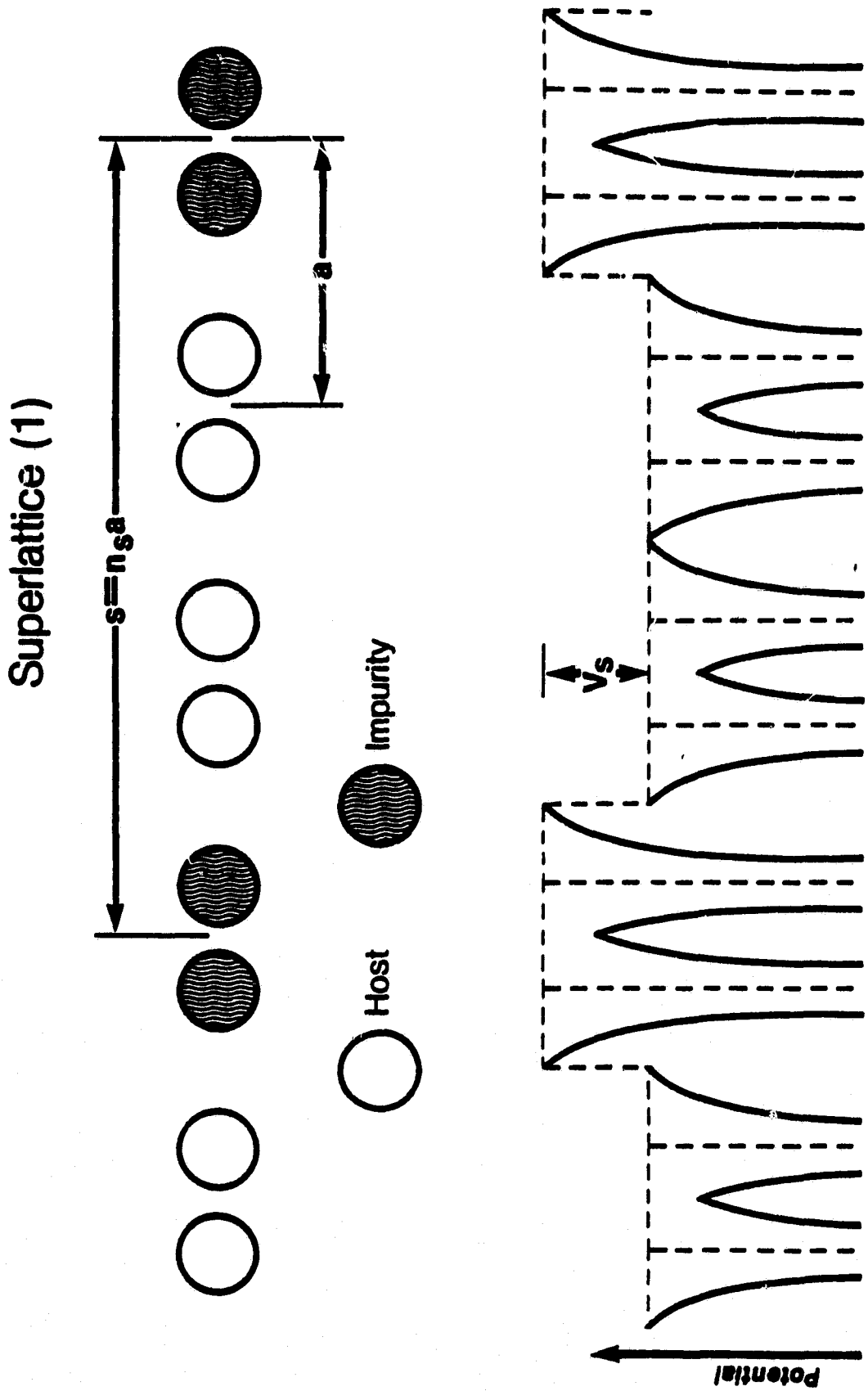

Fig. 1.

In order to treat the electronic structure of superlattices (1) and (2), an appropriate LCAO (linear combination of atomic orbitals) approach was developed. This technique was adopted both for its basic simplicity and because of the important relevance of the LCAO method to real tetrahedrally-bonded solids like silicon,[17] as discussed in Sec. II B below. In our LCAO description, a minimal basis set of two atomic-like orbitals, $|\alpha>$ and $|\beta>$, was chosen. These orbitals were assumed to be orthonormal and both of s symmetry. If the bond length is a/2 in superlattice (1) and $\sqrt{2}$ a/2 in superlattice (2), each host atom experiences equivalent nearest-neighbor interactions. Neglecting distant-neighbor couplings, this leads to five basic LCAO parameters for the host atoms: two diagonal energies

$$\varepsilon_\alpha = <\alpha|H|\alpha> \tag{4}$$

and

$$\varepsilon_\beta = <\beta|H|\beta> \ ; \tag{5}$$

and three interatomic matrix elements

$$V_{\alpha\alpha'} = <\alpha|H|\alpha'>, \tag{6}$$

$$V_{\beta\beta'} = <\beta|H|\beta'>, \tag{7}$$

and

$$V_{\alpha\beta'} = <\alpha|H|\beta'>, \tag{8}$$

where the prime denotes that the orbital is centered on a different site. For the impurity atoms, ε_α and ε_β are shifted to

$$\varepsilon_\alpha' = \varepsilon_\alpha + V_s \tag{9}$$

and

$$\varepsilon_\beta' = \varepsilon_\beta + V_s, \tag{10}$$

while $V_{\alpha\alpha'}$, $V_{\beta\beta'}$ and $V_{\alpha\beta'}$ remain unchanged. The host electronic structure (V_s=0) is established by a (4 x 4) secular determinant which may be solved analytically for the energy bands E(k). Our approach was to arbitrarily fix the five LCAO parameters at convenient values and study the change in the electronic structure as the superlattice parameters V_s, n_s and n_b were varied. The LCAO parameters adopted were

$$\varepsilon_\alpha = 2V, \tag{11}$$

$$\varepsilon_\beta = 6V, \tag{12}$$

and

$$V_{\alpha\alpha'} = V_{\beta\beta'} = V_{\alpha\beta'} = -V, \tag{13}$$

where

$$V = r\frac{\hbar^2}{2m}\left(\frac{\pi}{a}\right)^2 \tag{14}$$

is the natural unit of energy and r is a dimensionless scaling constant. These parameters lead to symmetrical valence and conduction bands with a direct band gap of magnitude E^g located at the zone center (k=0) in both superlattices (1) and (2). The matrix element $V_{\alpha\beta'}$ insures coupling between the valence and conduction bands and a finite E^g which scales directly with r. The corresponding valence-and conduction-band-edge effective masses are equal in this model,

$$m_h^* = m_e^* = m, \tag{15}$$

and scale as 1/r. The host values of E^g and m*/m for the cases of interest are summarized in Table I.

The superlattice band structure here is determined by a ($2n_p$ x $2n_p$) secular determinant which can only be solved numerically in general. A full computer program for this purpose has been developed and was used to obtain the results discussed below. Within the confines of the above model, the electronic structure of

Table I. Parameters of the model hosts in superlattices (1) and (2) for the choice of parameters $\varepsilon_\alpha = 2V$, $\varepsilon_\beta = 6V$ and $V_{\alpha\alpha'} = V_{\beta\beta'} = -V$, where $V = r\frac{\hbar^2}{2m}\left(\frac{\pi}{a}\right)^2$.

Superlattice	$V_{\alpha\beta'}$	E^g	m^*/m
(1)	0	0	$0.405\frac{1}{r}$
(1)	-V	1.66V	$1.384\frac{1}{r}$
(2)	-V	0.94V	$1.919\frac{1}{r}$

superlattices (1) and (2) was studied as a function of the parameters V_s, n_s and n_b. Calculations on superlattice (1) were performed over the parameter ranges

$$0 \leq V_s/V \leq 4.0, \tag{16}$$

$$2 \leq n_s \leq 8, \tag{17}$$

and

$$1/8 \leq n_b/n_s \leq 1/2. \tag{18}$$

The secular determinant in superlattice (1) is $(4n_s \times 4n_s)$ and hence varied from (8 x 8) to (32 x 32) over the range of n_s given in Eq. (17). Typical results for the superlattice energy bands are plotted in Fig. 2 for the case $n_s = 2$ and $n_b = 1$ and five values of V_s/V. The far left-hand panel shows the host bands folded into the minizone of the superlattice. As V_s is increased from zero, the host energy bands are separated, narrowed, and pushed up in energy with "minigaps" formed at the minizone boundaries. The quantitative magnitude of these effects, however, is clearly band dependent. As the size of the minigaps increases, the narrowed superlattice energy bands may in some cases being to be pushed towards one another leading to new strong interactions. In Fig. 2 this can be seen to occur for the lowest lying conduction band and the highest lying valence band. The superlattice band gap closes continuously as the strength of the superlattice potential V_s is increased. As illustrated in Figs. 3 and 4, the band gap closes more quickly with V_s when n_s is raised for fixed n_b or when n_b/n_s is raised for fixed n_s.

The corresponding band-edge effective mass m* is also found to vary rapidly with V_s. Initially, m* increases sharply because both the valence and conduction bands are flattened, but as E^g becomes smaller the bands interact strongly and m* decreases to a minimum value as $E^g \to 0$. This behavior is shown in Fig. 5

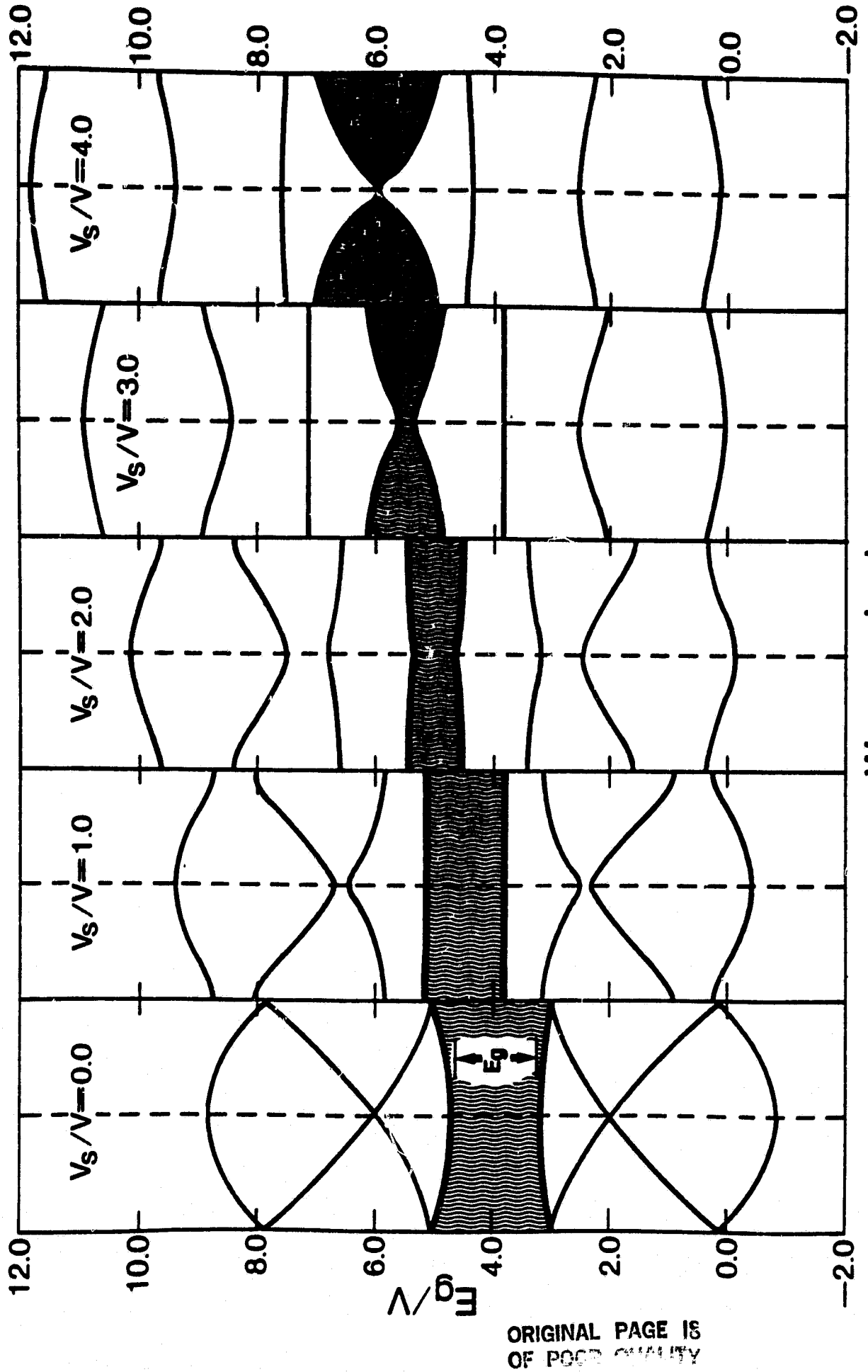

Fig. 2.

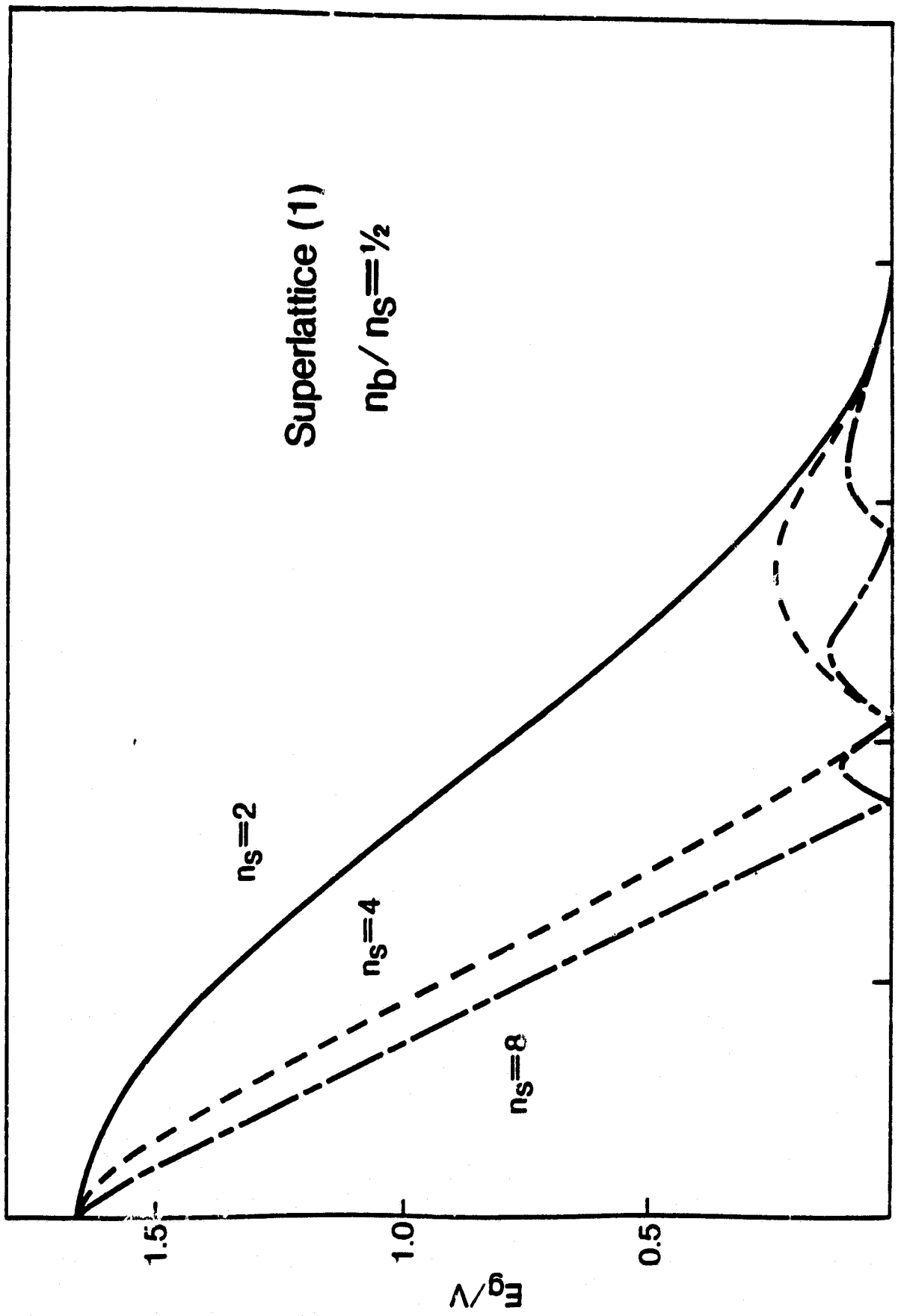

Fig. 3.

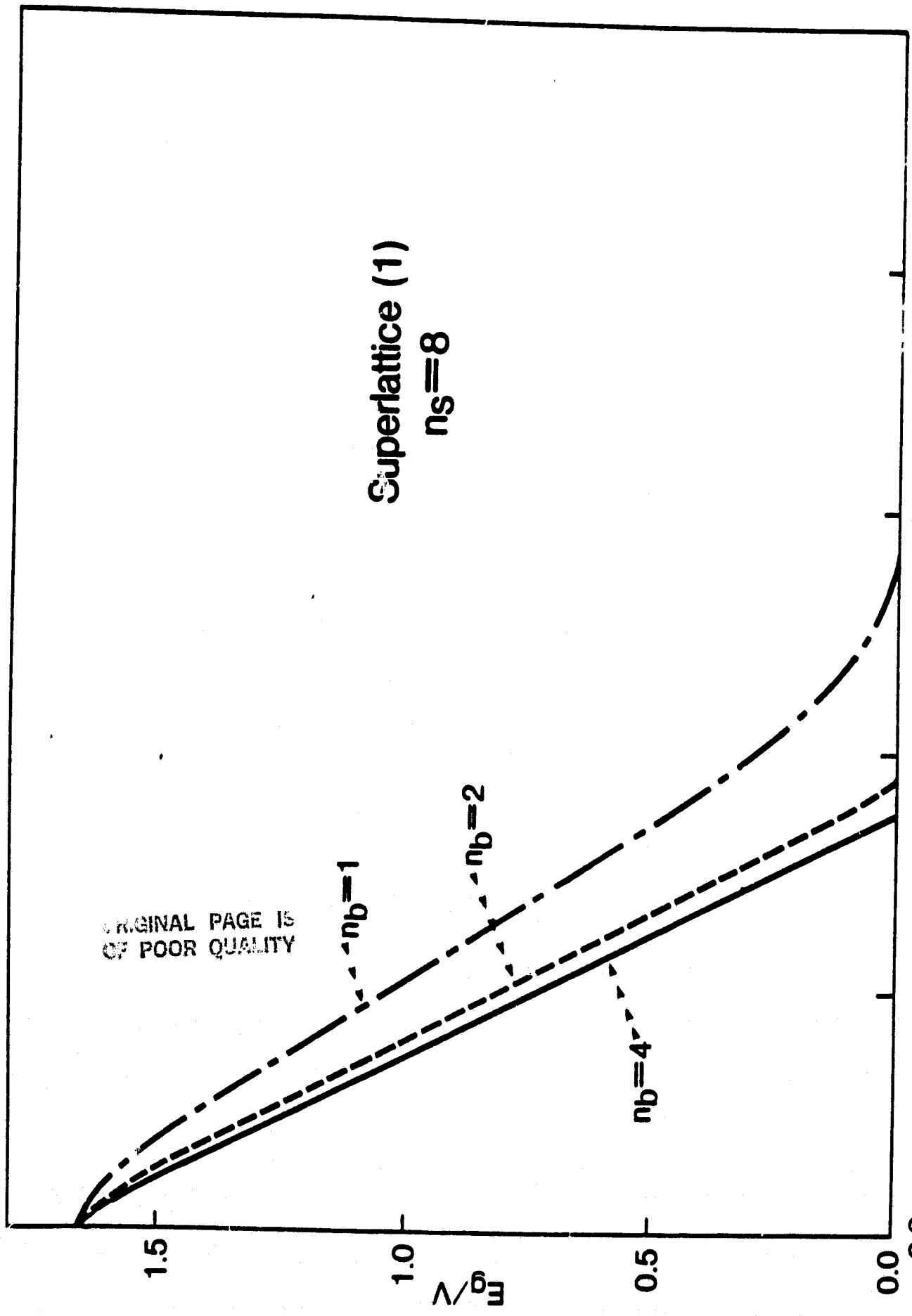
Superlattice (1)
n_s=8
n_b=1
n_b=2
n_b=4
E_g/V
V_s/V
0.0
0.5
1.0
1.5
2.0
3.0
4.0
ORIGINAL PAGE IS
OF POOR QUALITY

Fig. 4.

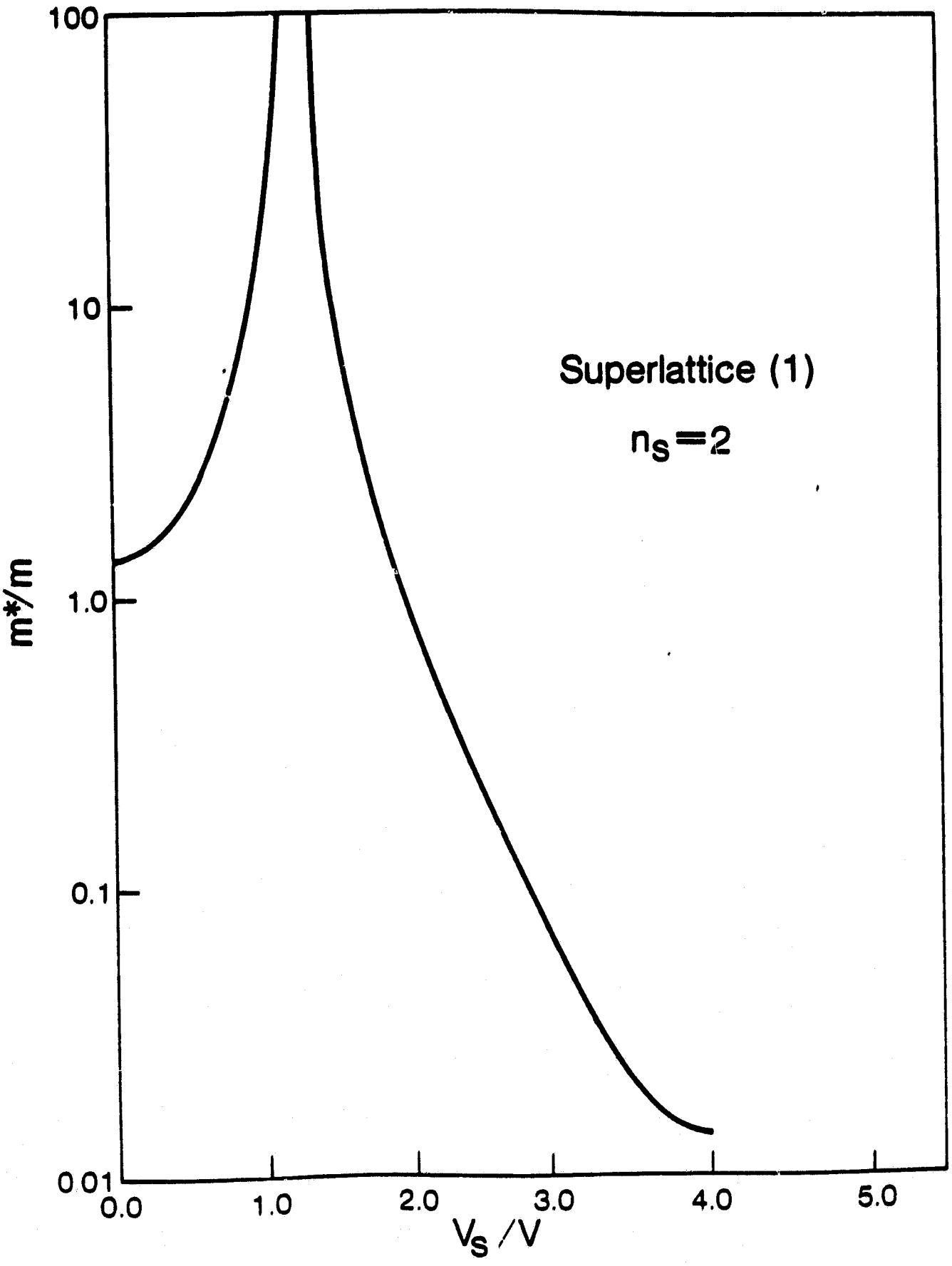

Fig. 5.

for the case $n_s = 2$ and $n_b = 1$ (and $r = 1$). More rapid variations occur as either n_s is increased for fixed n_b or as n_b/n_s is increased for fixed n_s. The actual minimum m* achieved at band-gap closing increases with n_s and also slightly with n_b/n_s. Thus small values of effective mass (and hence high carrier mobilities) can only be achieved for relatively strong superlattice potentials. To obtain $m^*/(m^*_{host} = 1.384) < 0.2$, one requires $V_s > E_g^{host} = 1.66$V in all cases studied with this model.

Saturation of the above effects occurs rapidly as n_s increases. In the hypothetical limit $n_s \to \infty$, one expects the band gap to first close when

$$V_s = E_g^{host} = 1.66 \text{ V}, \tag{19}$$

the value of the superlattice potential which would move the valence-band edge of the host to the position of the conduction-band edge. This value of V_s is only slightly less than the one we have obtained for $n_s = 8$, so that we expect little significant change in the above results for $n_s > 8$.

In the case of superlattice (2), we have considered structures with both square (SQR) and face-centered (FC) two-dimensional symmetry. The symmetry and dimensions of the real-space superlattices and the reciprocal-space minizones are illustrated in the left-and right-hand portions of Fig. 6, respectively. The effective superlattice constant is again $s = n_s a$. In the SRQ superlattice, the number of atoms per primative cell is

$$n_p = 2n_s^2, \tag{20}$$

while in the FC superlattice one has

$$n_p = n_s^2. \tag{21}$$

The maximum fraction of impurity atoms in the primative cell is 1/4 for the SQR configuration, but still 1/2 for the FC configuration, as it is for superlattice (1). The size of the secular determinant to be solved for the electronic

Superlattice (2)

Square:

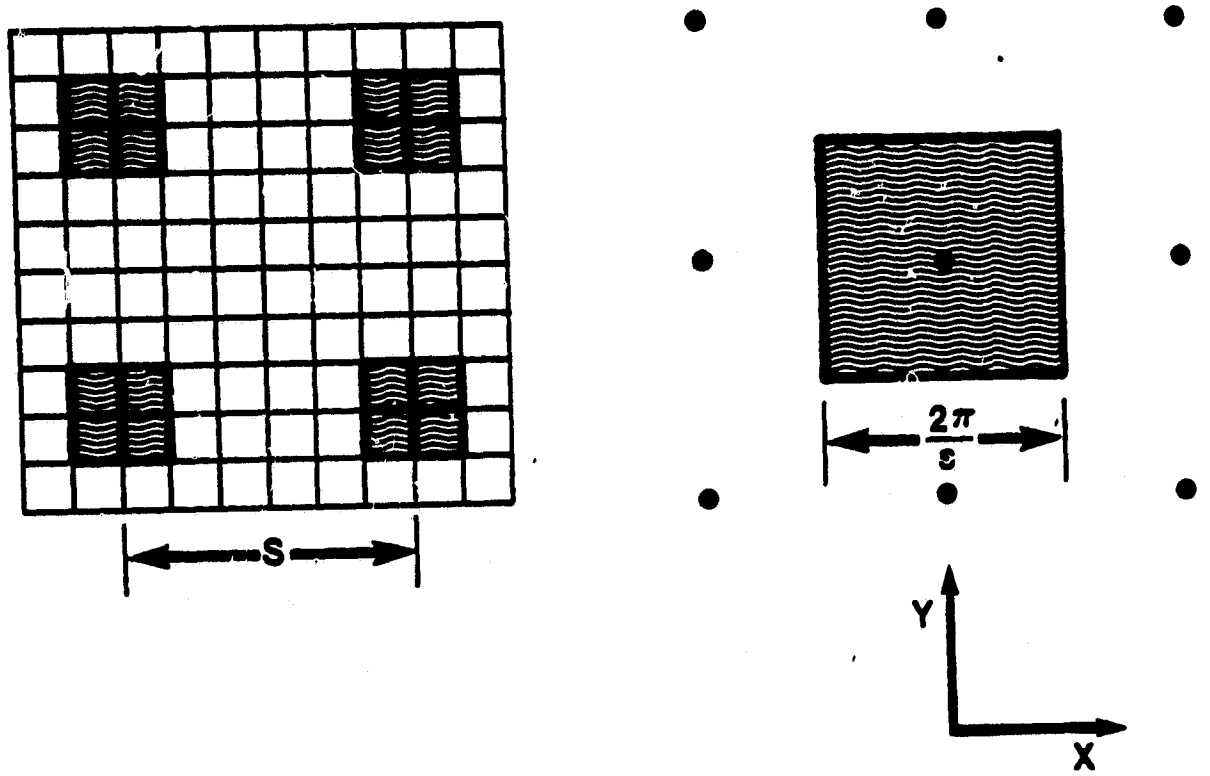

Face-Centered:

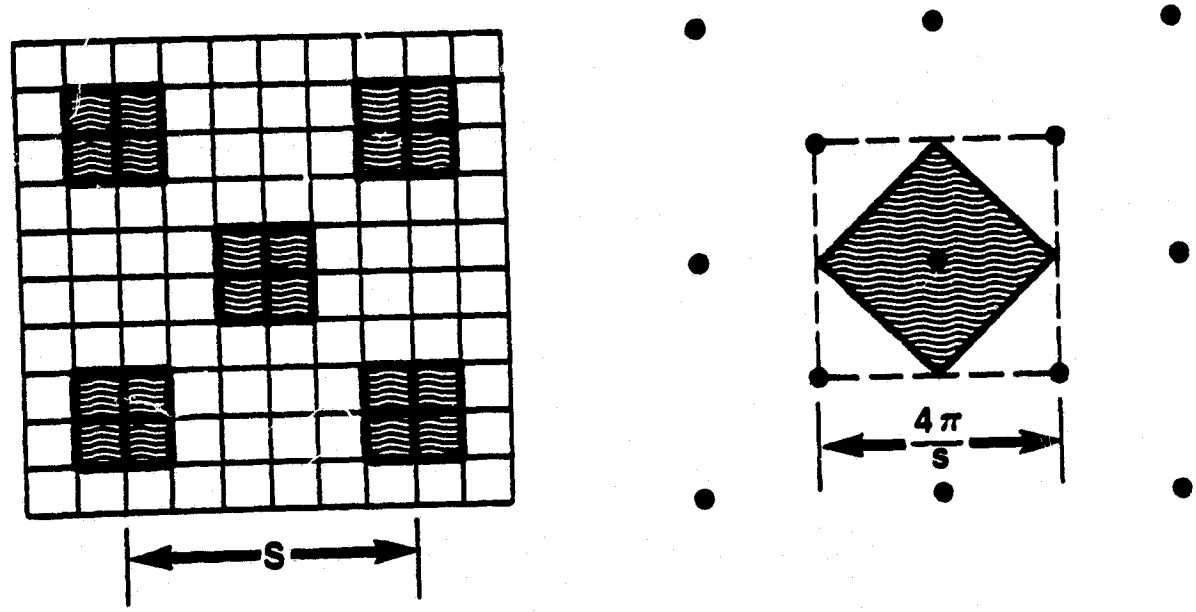

Fig. 6.

structure is now increased to $(4n_s^2 \times 4n_s^2)$ and $(2n_s^2 \times 2n_s^2)$, respectively.

We have performed calculations on the SQR and FC cases of superlattice (2) over the parameter ranges

$$0 \leq V_s/V \leq 5.0, \tag{22}$$

$$2 \leq n_s \leq 4, \tag{23}$$

and

$$1/8 \leq n_b/n_s \leq 1/2. \tag{24}$$

The behavior of the energy bands with varying V_s, n_s and n_b show basic similarities with that of superlattice (1), but a few noteworthy differences as well. There is again a continuous closing of the fundamental band gap as V_s is increased from zero in all cases considered except FC, $n_s = 2$, $n_b = 1$, where the gap first broadens slightly for small V_s. This behavior is shown in Fig. 7. As in the case of superlattice (1), the rate at which E^g approaches zero generally increases with n_s and the fraction of impurity atoms in the primative cell, n_b/n_p. In this regard, the FC congifuration is clearly more efficient than the SQR one because n_b/n_p is larger for given values of n_s and n_b. Unlike superlattice (1), however, the nature of the fundamental band gap (direct or indirect) can change as V_s is increased. In superlattice (1), the gap is direct at k=0 for all values of V_s. In superlattice (2), the gap is direct at k=0 only for small V_s. One or more changes to either an indirect gap (indicated by an arrow and a numeral II in Fig. 7) or to a direct gap away from the zone center (indicated by an arrow and a numeral I in Fig. 7) occur in every case. In addition, when a band edge moves away from k=0, both longitudinal and transverse effective masses arise. Only the longitudinal masses were investigated in detail and these were found to depend on V_s in much the same manner as m^* in superlattice (1).

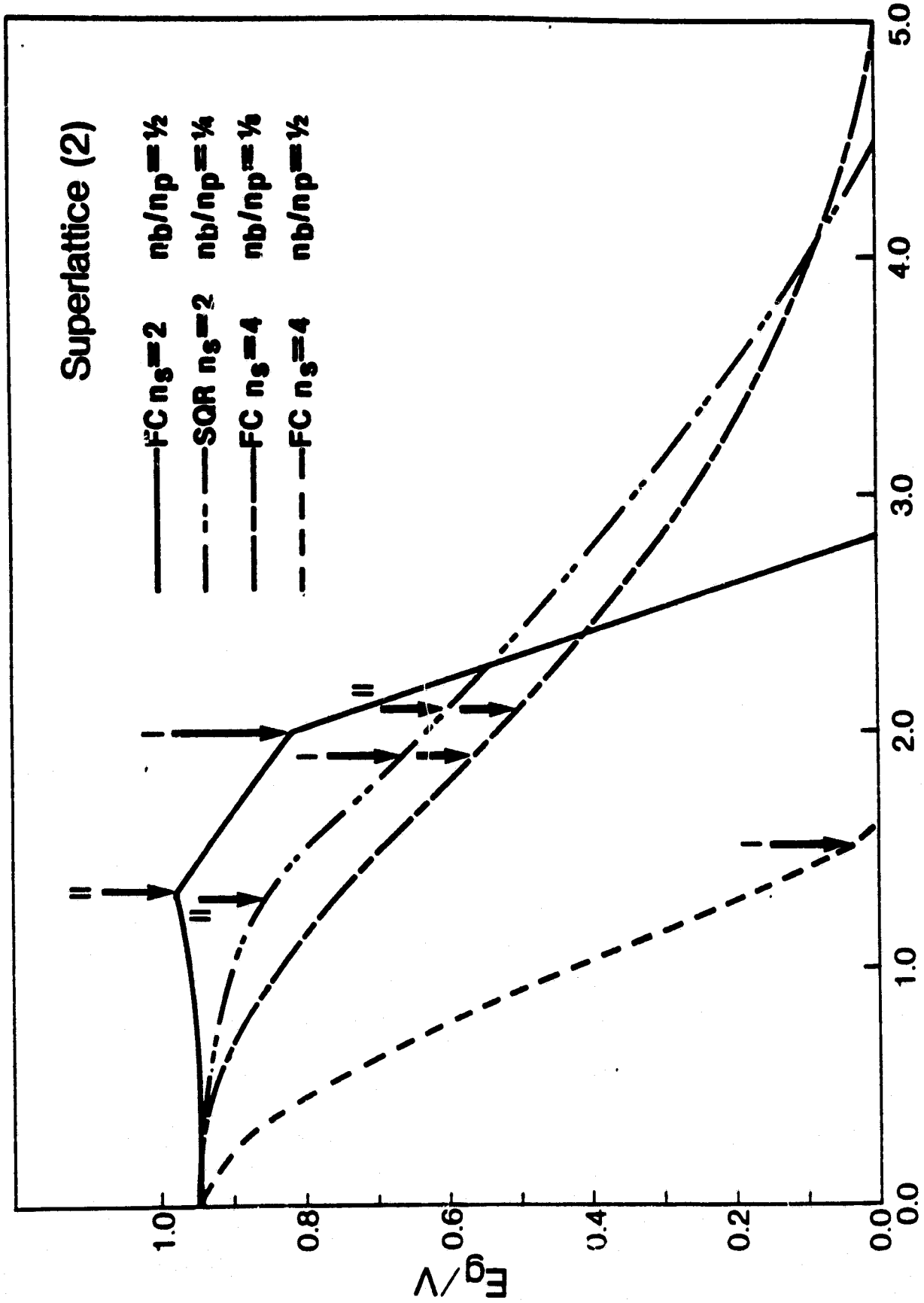
Superlattice (2)
FC n_s=2 nb/np=½
SQR n_s=2 nb/np=¼
FC n_s=4 nb/np=⅛
FC n_s=4 nb/np=½
I
II
E_g/V
V_S/V
0.0
0.2
0.4
0.6
0.8
1.0
1.0
2.0
3.0
4.0
5.0

Fig. 7.

B. Electronic Structure of One-Dimensional Silicon Superlattices

In superlattice (3), we replaced the simple model host by a full three-dimensional diamond structure. The superlattice itself was formed by replacing adjacent pairs of (100) planes of silicon atoms with impurity atoms, so that the periodicity in the y and z directions is unchanged, but in the x direction becomes

$$s = n_s \frac{a}{2}, \tag{25}$$

where a is the host silicon lattice constant which is assumed to stay fixed. In addition, we chose n_s to be an even integer, so that the superlattice always has simple tetragonal symmetry and the number of atoms per primative cell is

$$n_p = 2n_s. \tag{26}$$

The minizone in reciprocal space is then in the shape of a square prism rotated 45° about the x axis, as shown in the bottom portion of Fig. 8.

The simple minimal-basis LCAO method discussed above had to be suitable generalized for superlattice (3). In real covalent semiconductors like silicon, a minimal basis set consists of one s-like and three p-like atomic orbitals. A careful study of the electronic structure of pure silicon revealed that in this basis one must retain both nearest-neighbor and second-neighbor interatomic interactions to obtain a satisfactory description of the energy bands in the vicinity of the fundamental energy-band gap. The interatomic matrix elements which enter the band structure calculation can always be written as linear combinations of the basic forms $V_{ss\sigma}$, $V_{sp\sigma}$, $V_{pp\sigma}$ and $V_{pp\pi}$. Furthermore, these quantities are primarily functions of bond length $d = \sqrt{3}\, a/4$ in the solid and, following Harrison,[17] may be expressed in the form

$$V_{\ell\ell'm} = \eta_{\ell\ell'm} \hbar^2/(md^2), \tag{27}$$

Superlattice (3)

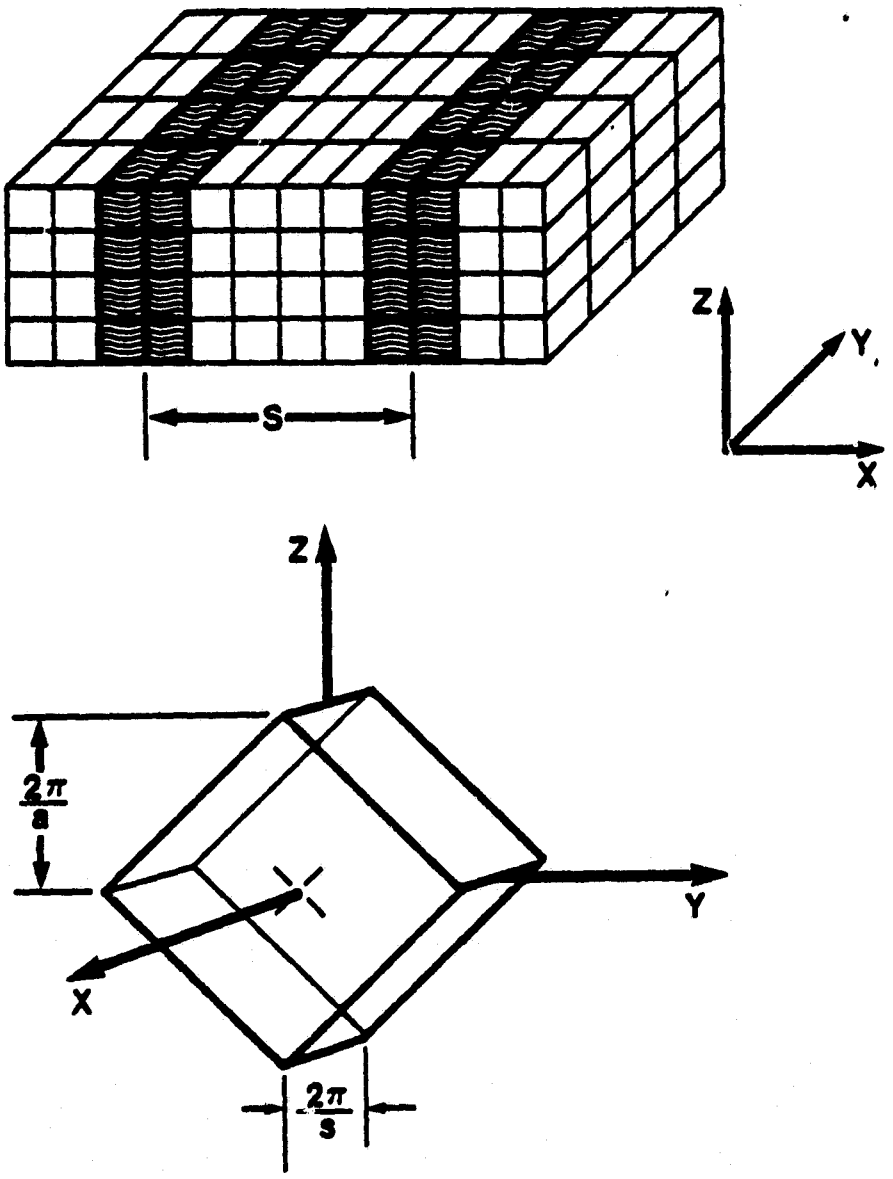

Fig. 8.

where ℓ,ℓ' = s or p and the subscript m is either σ or π. The dimensionless parameters $\eta_{\ell\ell'm}$ were fixed by an empirical fitting of the known pure silicon energy bands. The best set of values that we thereby obtained are listed in Table II.

As mentioned above, the bond length is assumed fixed when the superlattice is formed, so that the $V_{\ell\ell'm}$ are unchanged. The silicon intra-atomic energies ϵ_s and ϵ_p, on the other hand, become

$$\epsilon_s + V_s^{(s)} \tag{28}$$

and

$$\epsilon_p + V_s^{(p)} \tag{29}$$

for the substitutional impurity in the superlattice. Fitting of the bulk silicon bands gave a value $\epsilon_p - \epsilon_s = 4.786$ eV which also remains fixed. The effect of the superlattice potential is thus incorporated into two constants, $V_s^{(s)}$ and $V_s^{(p)}$, and represents, in general, a different potential seen by s and by p electrons. The special case

$$V_s = V_s^{(s)} = V_s^{(p)} \tag{30}$$

corresponds to the situation envisaged above in superlattices (1) and (2) where the impurity potential is rigidly raised or lowered by a constant value V_s. In the context of superlattice (3), we have designated this as type-I behavior. Another interesting limiting case occurs for

$$V_s = -V_s^{(s)} = V_s^{(p)} \tag{31}$$

in which case s and p electrons effectively see equal and opposite superlattice potentials. Detailed consideration of the electronic structure of Ge has suggested that this behavior, which we have designated as type-II, is to be expected in the Si-$Si_{1-x}Ge_x$ heterostructure superlattice. Our studies have further shown that a very approximate relation between the superlattice potential

Table II. Parameters $\eta_{\ell\ell'm}$ in Eq. (27) obtained from a best fit to the bulk silicon band gap

$\eta_{\ell\ell'm}$	Nearest neighbor	Second Neighbor
$ss\sigma$	-1.491	0.029
$sp\sigma$	1.308	0.051
$pp\sigma$	1.485	0.351
$pp\pi$	-0.276	-0.036

V_s and the Ge concentration x is

$$V_s = 0.5x \text{ (in eV)}. \tag{32}$$

Electronic structure calculations have been performed on superlattice (3) in both the longitudinal [100] direction and the transverse [001] direction in type-I as well as type-II cases over the parameter ranges

$$0 \leq V_s \leq 1.0 \text{ eV} \tag{33}$$

and

$$2 \leq n_s \leq 8 \tag{34}$$

In order to maximize the effective strength of the superlattice potential in each case, the ratio of impurity-layer to silicon-layer thickness was held constant at unity (corresponding to $n_b/n_s = 1/2$), as suggested by our model studies. For $n_s = 8$, this represents layers of about 11Å in thickness or a superlattice period of $s \cong 22$Å. Since the size of our secular determinant is $(8n_s \times 8n_s)$, direct calculation on thicker systems would require determinants larger than (64 x 64).

Typical results that we have obtained for the band structure in the vicinity of the fundamental energy gap are illustrated in Fig. 9. The top panel shows the pure silicon bands with the characteristic indirect gap and conduction band edges along the <100> directions out toward the zone boundaries. The center panel shows the effect of folding the bands back into the $n_s = 4$ minizone for $V_s = 0$. Four of the conduction-band minima remain fixed, but the remaining two along the [100] and [$\bar{1}$00] directions are displaced to positions near k = 0. When the suplerlattice potential V_s is increased from zero, the bands split apart, the fundamental gap closes and the [100] and [$\bar{1}$00] minima are further displaced, as shown in the bottom panel of Fig. 9. For the case illustrated (V_s = 0.5eV; type-II), the minima in fact have moved to the

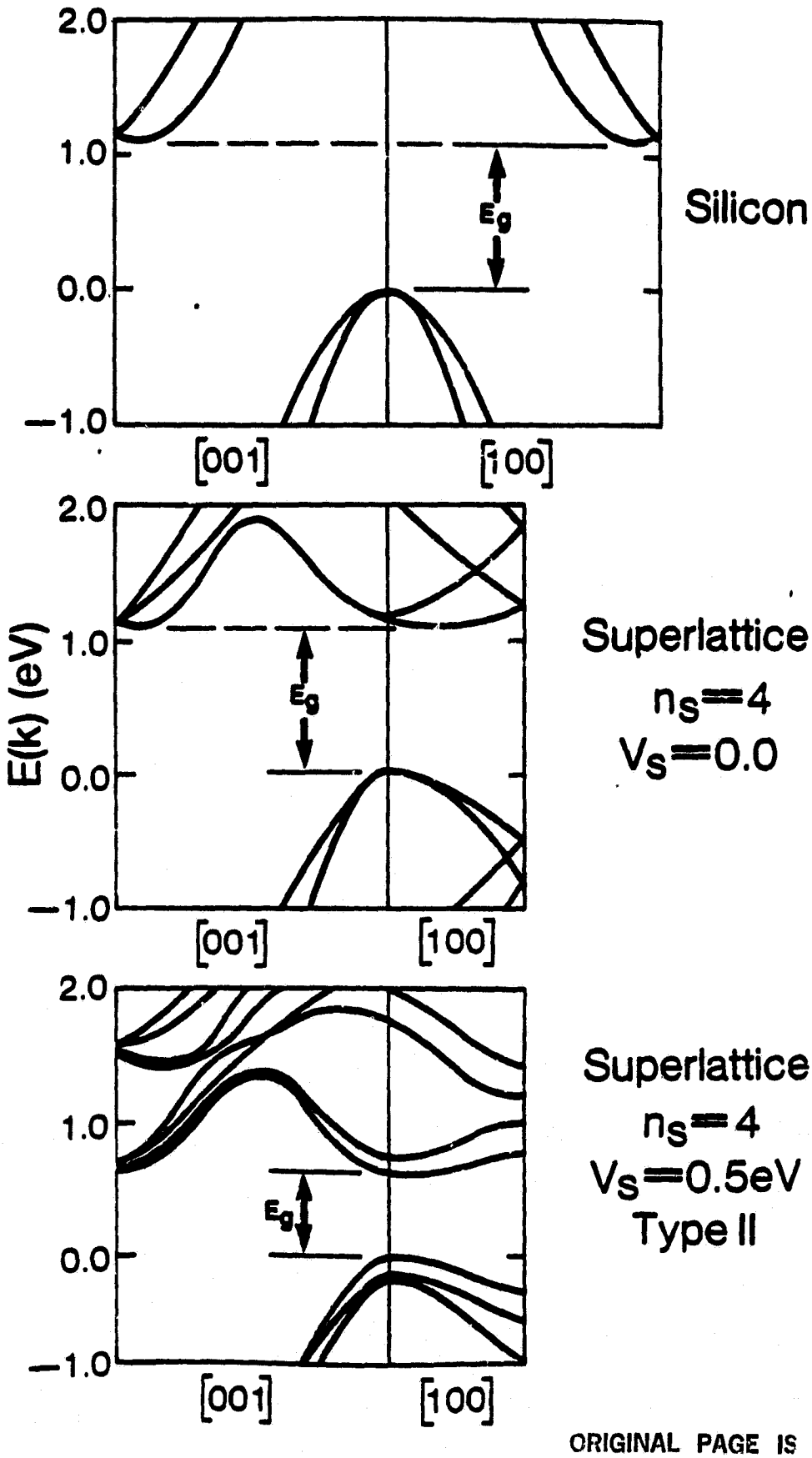

Fig. 9.

zone center and the gap has become direct.

As expected from our model superlattice studies, the fundamental band gap was found to decrease continuously as V_s is increased in all cases. The rate of change with V_s is significantly faster in the type-II case than in the type-I case, as shown in Fig. 10 for $n_s = 2$. This is to be expected on the basis of Eqs. (28)-(31), since the s and p energies are pushed together in the impurity layers for the type-II superlattice. The band gap in the type-I case remains indirect over the entire parameter range of Eqs. (33) and (34). In the type-II case, on the other hand, there is a tendency for the gap to become direct (at the zone center) for large V_s, as can be seen in Figs. 9-11. (In Figs. 10 and 11, the region between the arrows is that for which the gap is direct at $k = 0$). Also as in the model studies, the gap E^g was found to decrease more rapidly with V_s as n_s is increased. This is shown in Fig. 11. The effect is not as large as in superlattice (1) (compare Fig. 11 with Fig. 3), nor, in fact, did we find any clear evidence of saturation as n_s was increased from 2 to 4 to 6 to 8. Presumably, saturation will occur, but evidently thicker layers must be examined to see its onset.

The band edge longitudinal and transverse effective masses in superlattice (3) display rather complicated behavior, in general, due to the indirect nature of the band gap. A clearer picture emerges by examining only the effective masses at the zone center $k = 0$. This k point, of course, marks the valence-band maximum in all cases and hence is appropriate to the actual hole effective mass in the superlattice. But $k = 0$ also marks the position of the conduction-band minimum in type-II superlattices for large V_s, as mentioned above, in which case this point is directly relevant to the electron effective mass. At $k = 0$ it was found that the longitudinal mass always increases while the

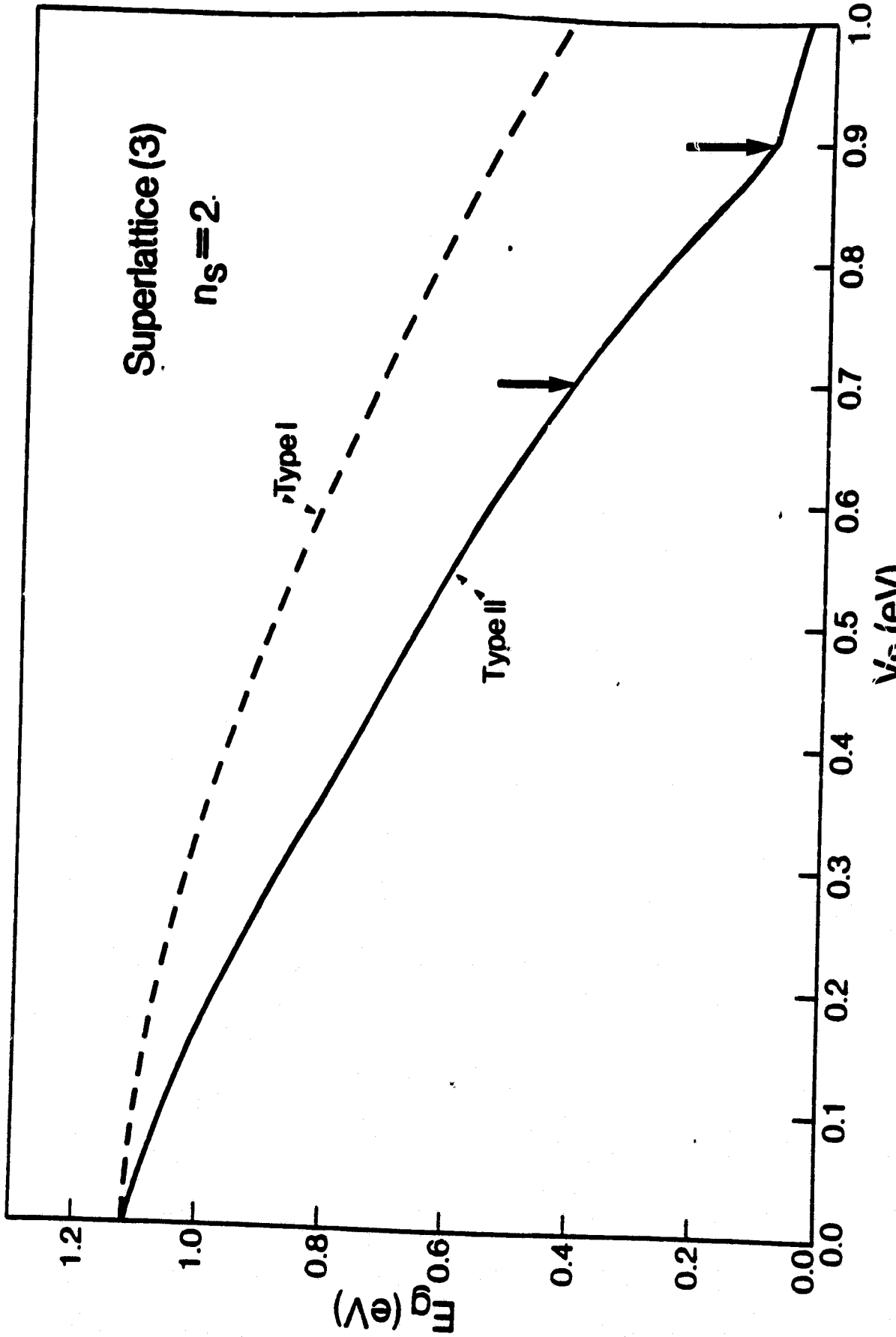
Superlattice (3)
$n_S = 2$
Type I
Type II
E_{fg} (eV)
V_S (eV)
0.0
0.2
0.4
0.6
0.8
1.0
1.2
0.1
0.3
0.5
0.7
0.9

Fig. 10.

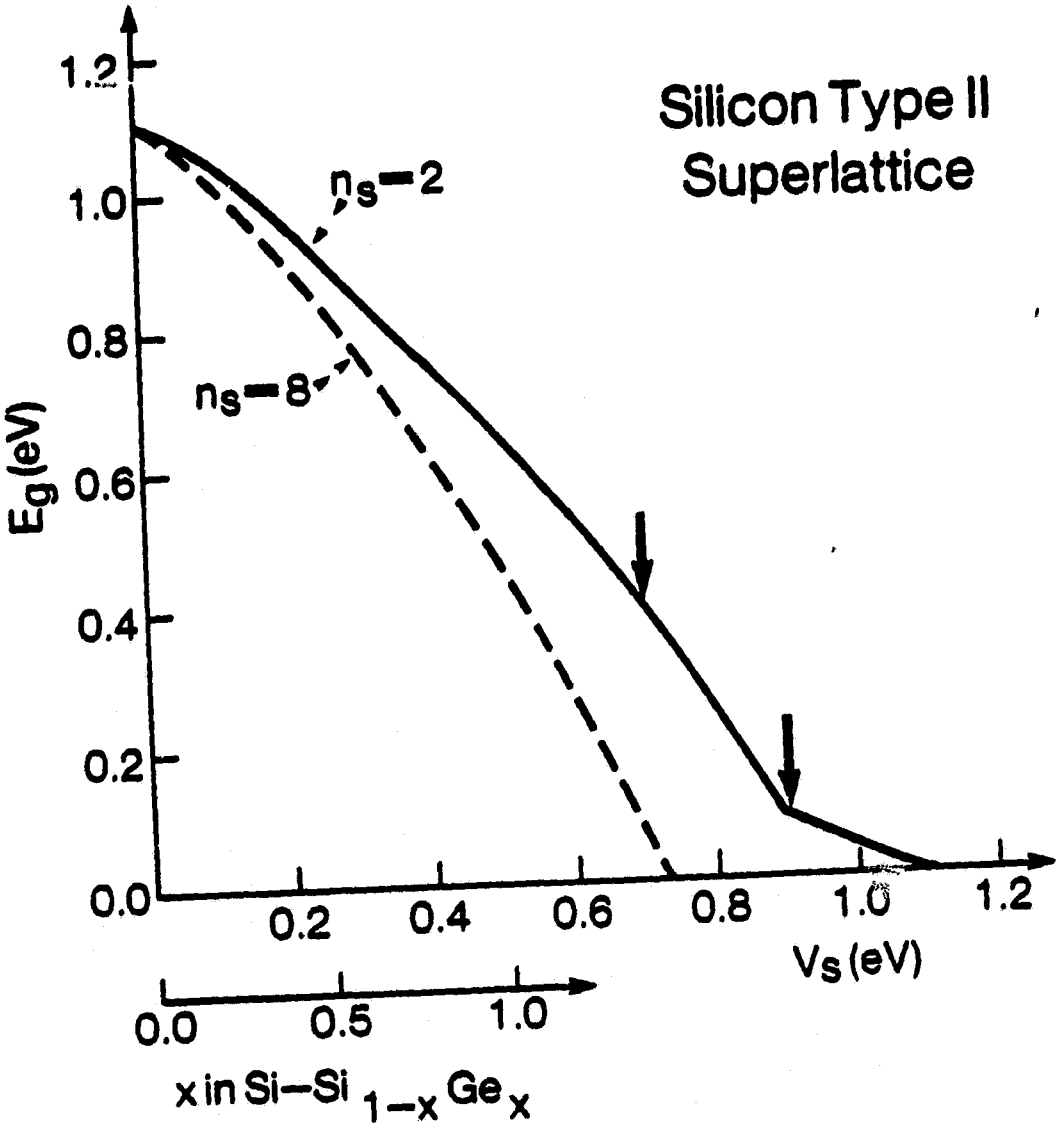

Fig. 11.

transverse mass decreases with increasing V_s. The former behavior is qualitatively in accord with our model studies, while the latter is a new three-dimensional effect and one which clearly bodes well for a mobility enhancement in the transverse direction. Details of the variation of the longitudinal and transverse hole masses, $m^*_{h\ell}$ and m^*_{ht}, with V_s are shown in Figs. 12 and 13. Figure 12 also illustrates the relatively stronger behavior in the type-II case than the type-I case. (The arrow denoting the cusps in the type-II curve in Fig. 12 marks the value of V_s beyond which the valence-band maxima moves away from $k = 0$.) As seen in Fig. 13, the initial rate of decrease of m^*_{ht} increases with n_s and hence layer thickness. While the net effect is not extremely large on the scale of the expected V_s in the Si-$Si_{1-x}Ge_x$ superlattice, saturation is again not yet in evidence and a bigger effect can be expected in thicker systems. (Note in Fig. 13 that the effective mass is given in units of the bulk silicon heavy-hole mass m^*_{hh}.)

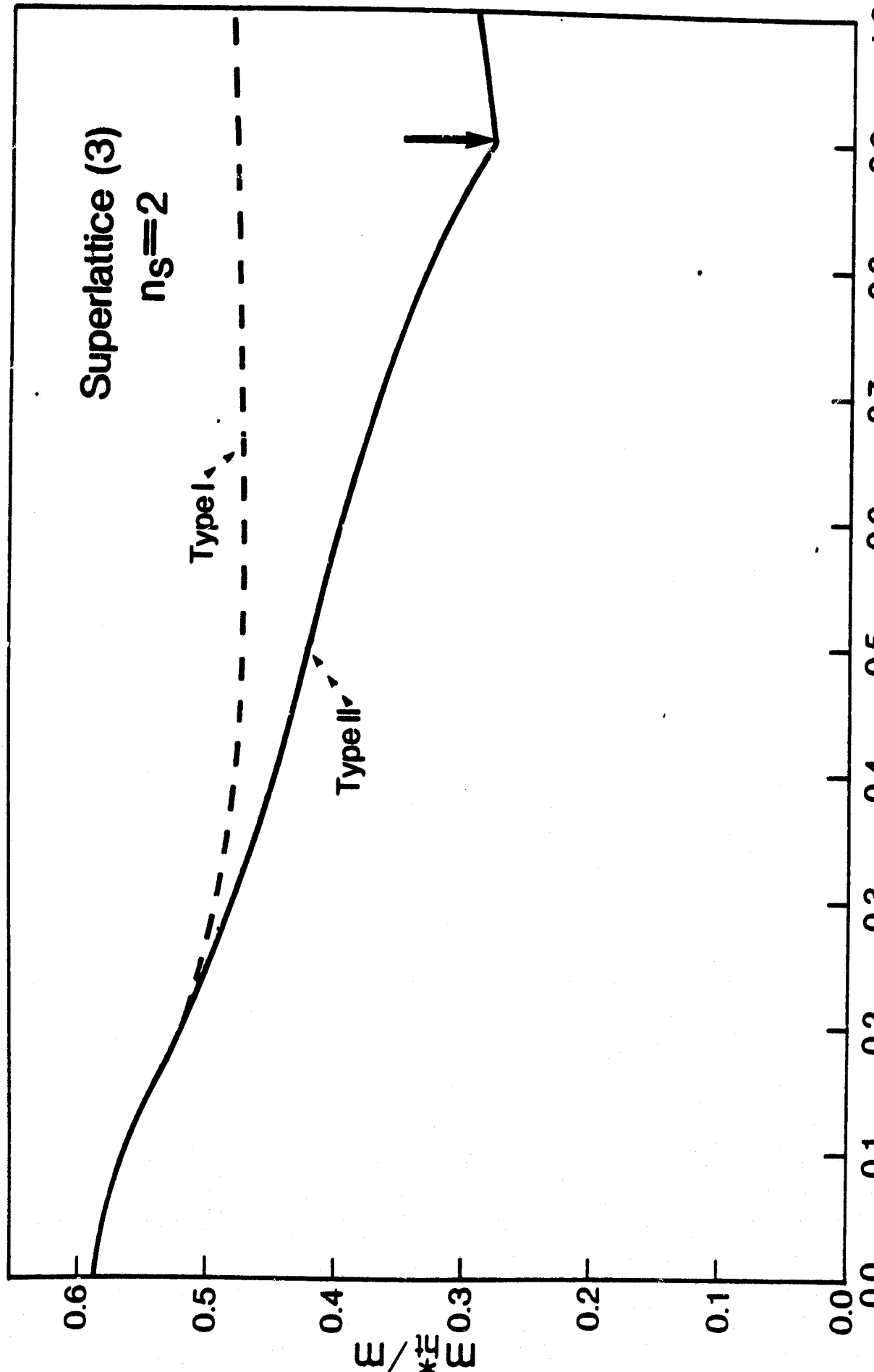
Superlattice (3)
n_S=2
Type I
Type II
Ξ^{**}_{11}/Ξ
V_S (eV)
0.0
0.1
0.2
0.3
0.4
0.5
0.6
0.7
0.8
0.9
1.0

Fig. 12.

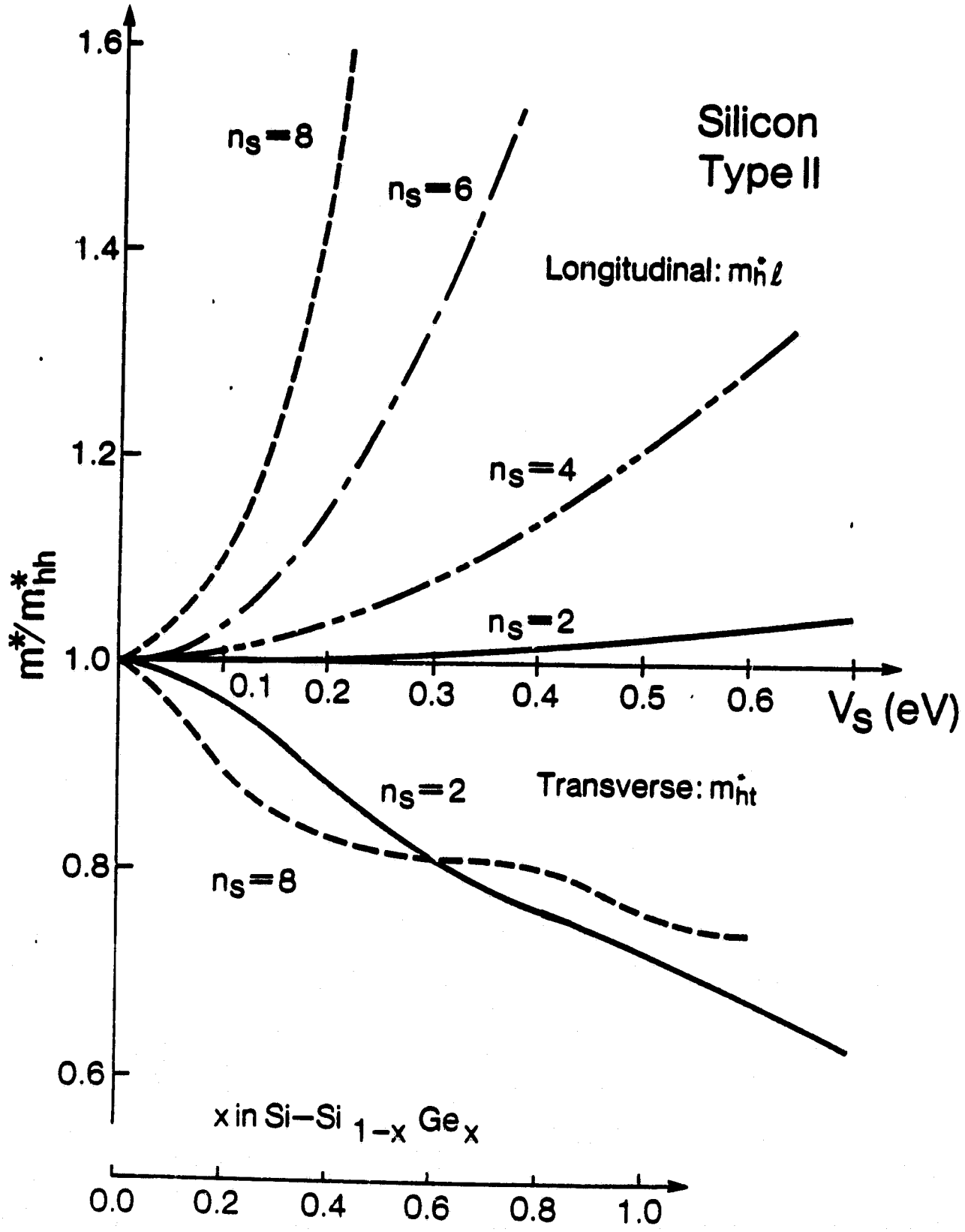

Fig. 13.

III. CONCLUSIONS

The theoretical studies described above have led to a number of useful findings and should greatly help focus the direction of future investigations on silicon superlattices. We have found a wide range of interesting behavior possible including the desirable features of smaller fundamental energy band gaps and reduced effective masses. Such effects correlate strongly with both the chemical (i.e., the magnitude of the superlattice potential V_s) and geometrical (i.e., layer thickness parameters n_s and n_b/n_s) nature of the superlattice. While details vary, the following general trends are in evidence:

(i) The effective strength of superlattice varies directly with V_s, n_s, and n_b/n_s. In one-dimensional silicon superlattices one can conveniently choose equal layer thicknesses to maximize n_b/n_s at 1/2. Saturation of the superlattice strength with increasing n_s (for fixed V_s) is expected and was found to occur rapidly in the model superlattices studied. In the real silicon superlattice, however, saturation effects were not observed for layer thicknesses up to 11 Å.

(ii) The fundamental band gap E^g of the superlattice continuously decreases with increasing superlattice strength. The direct or indirect nature of the gap can readily change in multi-dimensioned systems. In the real silicon superlattice, a definite trend toward a direct gap with increasing superlattice strength was observed.

(iii) The band-edge effective mass in the superlattice or longitudinal direction initially increases with increasing superlattice strength. As shown in the model superlattice studies, only for very large (and probably physically inaccessible) V_s can the trend be reversed and the longitudinal mass be made to decrease below its value for $V_s = 0$.

(iv) The band-edge effective mass in the transverse direction, on the other hand, decreases with increasing superlattice strength. In the real silicon superlattice studied, the effect was found to increase with increasing layer thickness.

Future theoretical work on silicon superlattices will investigate thicker-layer silicon systems as well as variable orientations (i.e., [110] and [111] as well as [100]) of the superlattice. Thick-layer calculations, however, will require modifications in the theoretical methods used here. Promising wave-function-matching techniques are currently being developed in the context of III-V semiconductor superlattices.[18-20] Such methods should have applicability to silicon superlattices.

A complementary experimental program aimed at studying Si-$Si_{1-x}Ge_x$ superlattices has recently been initiated at Rockwell International and preliminary results do show an enhanced electron mobility in the transverse direction.[21] In light of our findings, it would be extremely interesting to investigate whether or not this arises from a decreased transverse effective mass.

Some of work described in Sec. II B of this report was presented at the 1981 March Meeting of the American Physical Society held in Phoenix, Arizona.[22] A paper summarzing this research is also currently in preparation.[23]

IV. REFERENCES

1. L. Esaki and R. Tsu, IBM J. Res. Dev. 14, 61 (1970).
2. L. Esaki and L.L. Chang, Crit. Rev. Solid State Sci. 6, 195 (1976).
3. L. Esaki and L.L. Change, Phys. Rev. Lett. 33, 495 (1974).
4. R. Tsu, A. Koma and L. Esaki, J. Appl. Phys. 46, 842 (1975).
5. R. Dingle, Festkorperprobleme 15, 21 (1975).
6. R.D. Dupius, R.D. Dapkus, N. Holonyak, Jr., E.A. Rezek and R. Chin, Appl. Phys. Lett. 32, 295 (1978).
7. R.D. Dupius and P.D. Dapkus, Appl. Phys. Lett. 32, 406 (1978).
8. R.D. Dupius and P.D. Dapkus, Appl. Phys. Lett. 32, 473 (1978).
9. R. Dingle, H.L. Stromer, A.C. Gossard and W. Wiegmann, Appl. Phys. Lett. 33, 665 (1978).
10. T. Ando and S. Mori, J. Phys. Soc. Japan 47, 1518 (1979).
11. S. Mori and T. Ando, J. Phys. Soc. Japan 48, 865 (1980).
12. V. Narayanamurti, H.L. Stormer, M.A. Chin, A.C. Gossard, and W. Wiegmann, Phys. Rev. Lett. 43, 2012 (1979).
13. D.C. Tsui, H.L. Stormer, A.C. Gossard and W. Wiegmann, Phys. Rev. B 21, 1589 (1980).
14. C. Colvard, R. Merlin, M.V. Klein and A.C. Gossard, Phys. Rev. Lett. 45, 298 (1980).
15. W. Andreoni and R. Car, Phys. Rev. B 21, 3334 (1980).
16. R. Dingle, A.C. Gossard and H.L. Stormer, Bell Labs. Record 58, 274 (1980).
17. W.A. Harrison, Electronic Structure and the Properties of Solids (Freeman, San Francisco, 1980).
18. J.N. Schulman and T.C. McGill, Solid State Commun. 34, 29 (1980).
19. S.R. White and L.J. Sham, Bull. Am. Phys. Soc. 26, 390 (1981) and to be published.

20. Y.C. Chang and J.N. Schulman, Bull. Am. Phys. Soc. 26, 391 (1981) and to be published.

21. A.B. Jones (private communication).

22. J.A. Moriarty, Bull. Am. Phys. Soc. 26, 421 (1981).

23. J.A. Moriarty (to be published).